Title

Sum-frequency spectroscopy and imaging of aligned helical polypeptides

Journal

IEEE Journal of Selected Topics in Quantum Electronics, 10(5)

ISSN

1077-260X

Authors

Knoesen, A
Pakalnis, S
Wang, M
et al.

Publication Date

2004-09-01

Peer reviewed

Sum-Frequency Spectroscopy and Imaging of Aligned Helical Polypeptides

André Knoesen, *Senior Member, IEEE*, Saulius Pakalnis, Mingshi Wang, William D. Wise, Nancy Lee, and Curt W. Frank

***Abstract*—The sum-frequency spectroscopy signatures of NH- (amide A) and C = O (amide I) groups, the amide segments in all proteins, are measured in thin films that consist of an ensemble of right-handed, helical poly-γ-benzyl-L-glutamate (PBLG) macromolecules that are endgrafted and self-organized into a monomolecular film with a large degree of unidirectional order. Distinct sum-frequency spectral signatures associated with the amide A and the amide I bands are observed because of a strong noncentro-symmetry produced by intra- and intermolecular forces. Hydrogen bonding self-organizes amino and acidic groups within the molecular helical scaffold. In an endgrafted thin film, repulsive electrostatic forces between PBLG macromolecules stabilize the organization between molecules. The average orientation of the PBLG chain was measured. Imaging scans using sum-frequency generation, complemented by atomic force microscopy, were used to investigate the uniformity of orientation of the PBLG chains.**

***Index Terms*—Biological materials, image generation, nonlinear optics, spectroscopy.**

I. Introduction

PROTEINS play an essential physical and chemical role in living systems and consist of chains of interconnected molecular structures known as amino acids. The amino acids form linear chains along with side chains (e.g., glutamine, asparagines, tyrosine, etc.) create polypeptides that characterize a particular protein. Polypeptides are the building blocks that self-assemble into structures that can have a high degree of order with interesting nonlinear optical properties.

Second harmonic generation was observed at least four decades ago in crystals of amino-acids and collagen protein structures [1], [2] indicating that noncentrosymmetric order can exist within proteins. The first quantitative study of protein molecules was performed by Bethea and Levine [3] soon after they developed the electric field induced second-harmonic (EFISH) technique to quantify the microscopic second-order (β) and third-order (γ) hyperpolarizability of organic molecules [4]. They studied a homopolypeptide molecule poly-γ-benzyl-L-glutamate (PBLG). While such synthetic proteins lack the complexity of naturally occurring proteins, these poly(amino acids) or polypeptides exhibit the same secondary conformations as seen in proteins. PBLG stabilizes in an extended, rigid, α-helix configuration, resulting in unusual properties, such as a very large electrostatic dipole moment. A large dipole moment makes a molecule attractive for EFISH since the molecules are dissolved in a liquid and aligned with an electric field. Second harmonic generation has since been used to study cellular membranes [5]–[10] and is becoming a popular technique to image highly structured biological materials [6], [11]–[20].

In the last two decades, an in-depth understanding has developed of the origins of second-order effects in organic molecules and how noncentrosymmetric molecules can be arranged at the macroscopic level into noncentrosymmetric ordered films [21], [22]. This organization is either through self-assembly such as crystallization [23], or by directed assembly methods such as Langmuir–Blodgett–Kuhn deposition [24], layer-by-layer deposition [25]–[27], and, in the case of polymer films, electric field poling [28]. These methods of aligning molecules are quite different from those present in nature. For such reasons, we are interested in how the lack of inversion symmetry that is present at the molecular, intermolecular, and tissue level in biological materials is induced and how it leads to second-order nonlinear effects. It is interesting to note that the specific origin of the nonlinear effect in one of the most well-known protein structures to produce second harmonic generation, namely collagen, remains unknown [15].

Long-range orientational order in a material is probed by second harmonic measurements and complements the techniques used for short range orientational order such as X-ray diffraction and atomic force microscopy. Sum-frequency generation (SFG) vibrational spectroscopy specifically identifies the molecular groups that produce second-order nonlinear optical effects [29]. By temporally and spatially overlapping infrared (IR) and visible laser pulses on a sample under investigation, a sum-fregency signal is produced that is detected in the visible. If the IR wavelength matches the IR and Raman active resonant vibrational modes of a molecule [30] and its polarization is aligned to excite it, a resonance-enhanced signal is produced. Recently, SFG has been used to study proteins adsorbed at interfaces [31]–[33].

In this paper, we use, for the first time, SFG vibrational spectroscopy to identify the molecular origins of second-order effects in films of the synthetic protein PBLG. We also use SFG

Manuscript received December 18, 2003; revised August 10, 2004. This work was supported by the Material Research Science and Engineering Center (MRSEC) Program of the National Science Foundation under Award DMR-9808677 and Award DMR0213618, both given to the Center on Polymer Interfaces and Macromolecular Assemblies.

A. Knoesen, S. Pakalnis and M. Wang are with the Department of Electrical and Computer Engineering, University of California, Davis, CA 95616 USA (e-mail: knoesen@ece.ucdavis.edu).

W. D. Wise was with the Department of Electrical and Computer Engineering, University of California, Davis, CA 95616 USA. He is now with the Department of Physics, Massachusetts Institute of Technology, Cambridge MA 02139 USA.

N. Lee and C. W. Frank are with Department of Chemical Engineering, Stanford University, Stanford, CA 94305 USA.

Digital Object Identifier 10.1109/JSTQE.2004.837226

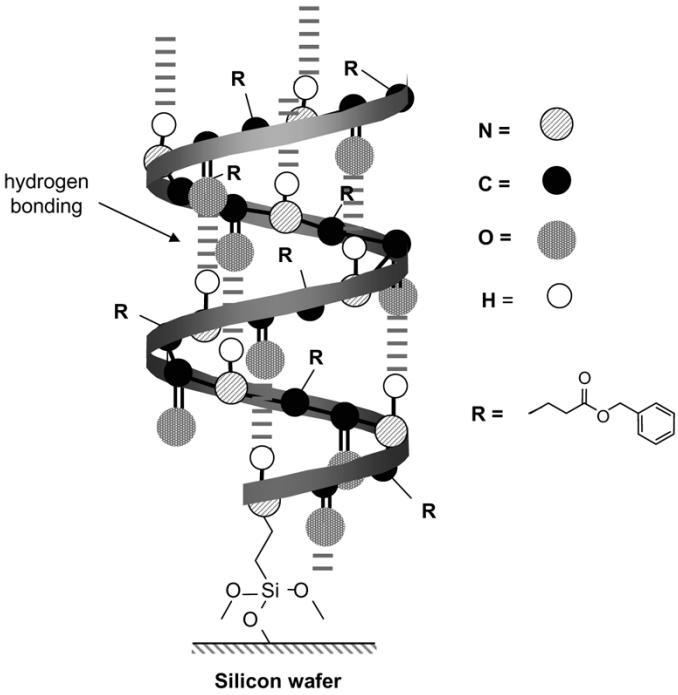

Fig. 1. Molecular structure of PBLG is a α-helix. The carbonyl (C = O) and amino (N-H) groups are oriented within the α-helical molecular scaffold by strong hydrogen bonding to produce a noncentro-symmetry at the molecular level.

to map the orientational order of a thin film of PBLG fabricated by endgrafting vapor phase deposition and show that the film has a high degree of long-range orientational order that extends over area of several millimeters square.

II. PBLG Molecules

The polypeptides assemble into a highly ordered three-dimensional supermacromolecular structure. A regular network is formed by intramolecular hydrogen bonding between the carbonyl and the amino N-H groups on the main chain, and sometimes the sidegroups. As shown Fig. 1, in PBLG the C = O group repeat unit i hydrogen bonds to the N-H group repeat unit $i+4$ to form a rigid α-helical molecular scaffold [34]. The polar alignment of these groups produces a net electrostatic dipole moment along the main axis of the molecule. Unlike a flexible chain polymer, the PBLG α-helix has a long persistence length. To a good approximation the net dipole moment is proportional to the number of peptide monomers N. The dipole moment of a PBLG molecule in dichloroethane was measured to be $\mu_{\mathrm{PBLG}} = \mathrm{N} \times 3.4$ Debye [3]. For PBLG with $\mathrm{N} = 2500$, electrostatic dipole moments have been reported in the 6000–8000 Debye range. For the PBLG molecules used in this paper, N is approximately 100, leading to an estimated dipole moment of 340 Debye. The second-order nonlinear properties are also dominated by the alignment of the C = O group with the N-H groups. The nonresonant second hyperpolarizibility of a PBLG molecule was estimated at $\beta_{\mathrm{PBLG}} = \mathrm{N} \times 8.3776 \times 10^{-41}$ m^4/V [3]. EFISH measurements have also been performed on PBLG with second-order nonlinear active sidegroups [35].

III. PBLG Monomolecular Films

Dipole-dipole interactions play an important role in how organic molecules assemble in second-order nonlinear thin films [36]. In assembling films of PBLG, given the large electrostatic dipole moment of the individual molecules, dipole–dipole interactions play a particular important role. In physisorbed PBLG films, such as deposited by Langmuir–Blodgett-Kuhn technique or spincoating, neighboring polypeptide helices form antiparallel pairs [34]. Solution evaporated PBLG films [37] and spincoated films of PBLG with second-order nonlinear active sidegroups [38] that have been electric field poled, also exhibit the energetically preferred antiparallel alignment of neighboring polypeptide helices.

Monomolecular PBLG films with a high degree of polar order can be prepared by covalently grafting the ends of PBLG molecules to a solid substrate. This is accomplished by first modifying the surface with initiators for subsequent the polymer synthesis, and then growing a helical chain that is tethered to the surface (*grafting from* approach) [39], [40]. Surface polymerization to produce PBLG monomolecular films has been performed in the melt [41], in solution [40], [42]–[45], and by a vapor deposition polymerization [46]. Vapor deposition polymerization was used in this paper to grow a PBLG film. The advantage of the vapor deposition method is that it is a solventless procedure; moisture and impurities from the solvent are eliminated, thus minimizing unwanted polymer intermediates. During the vapor deposition process, PBLG helices are grown that are chemically grafted to a silicon dioxide interface that has been previously functionalized with a primary amino group. The vapor deposited PBLG is right handed, which is determined by the fundamental structure of the poly(amino acid). All vapor-deposited poly(amino acids) fabricated to date, the secondary structure is qualitatively the same as observed in normal bulk conditions. During the fabrication process, physisorbed PBLG are dispersed between the chemically-grafted molecules, and they have their dipole moments oriented antiparallel to the chemically-grafted molecules. After the deposition process the film is aggressively washed, which presumably removes the loosely bound physisorbed molecules, because a significant increase in the polar order of the film is observed [34]. PBLG films with thicknesses up to 150 nm has been produced by vapor phase deposition. The thickness of the PBLG films used in this study was 30 nm. With only the chemically-grafted molecules present, with one end firmly attached to the interfaces, repulsive electrostatic forces exist between neighboring molecules, and as will be shown in this paper, these forces lead to a high degree of long-range order.

The electromechanical and electrooptic properties of end-grafted PBLG monolayer film have been investigated previously. Jaworek *et al.* studied the piezo-electric properties [47]. The field-induced change in film thickness were dominated by a inverse-piezoelectric effect and demonstrated that the helices were in a parallel arrangement. An electrooptic coefficient on the order of 0.3 pm/V was measured that exhibited no detectable dependence on frequency of the exciting ac field [34] indicative of a dominant electronic contribution to the second-order nonlinear properties. While such measurements

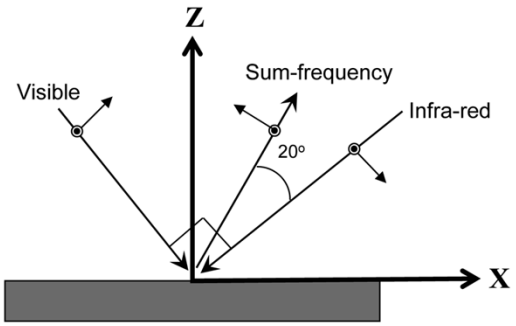

Fig. 2. Experimental arrangement of SFG spectroscopy experiment. The IR and the visible beam are kept at 90° with respect to each other. The polarization vectors of the s- and p-polarized waves are indicated in the figure. The reflected SFG beam's direction is determined by momentum conservation. As the wavelength of the IR pulse is changed, the sample is rotated around the Y axis to keep angle between the IR and the SFG beam at 20°, which keeps the SFG beam position on the detector constant.

are indicative of a strong polar order, the sum-frequency measurements in this paper provide the conclusive evidence for the polar order in end-grafted PBLG films.

IV. Sum-Frequency Analysis

An electric field $\vec{E}_{\rm SF}\ (t)$ is created by sum-frequency generation in a thin film from the interaction between two electric fields, one in the infrared $\vec{E}_{\rm IR}\ (t)$ and one in the visible $\vec{E}_{\rm VIS}\ (t)$, through second-order nonlinear polarization interactions. In the coordinate system shown in Fig. 2, $\vec{k}_{\rm IR}= -\kappa_1\hat{x} - \beta_1\hat{z}$, $\vec{k}_{\rm VIS}= \kappa_2\hat{x} - \beta_2\hat{z}$, $\vec{k}_{\rm SF}= \kappa_3\hat{x} + \beta_3\hat{z}$, and

$$\vec{E}_{\rm SF}\ (t) = {\rm Re}\left[\vec{E}\ (\omega_3)e^{-jk_{03}(\kappa_3 x+\beta_3 z)}e^{j\omega_3 t}\right]$$

$$\vec{E}_{\rm VIS}\ (t) = {\rm Re}\left[\vec{E}\ (\omega_2)e^{-jk_{02}(\kappa_2 x-\beta_2 z)}e^{j\omega_2 t}\right]$$

and

$$\vec{E}_{\rm IR}\ (t) = {\rm Re}\left[\vec{E}\ (\omega_1)e^{jk_{01}(\kappa_1 x+\beta_1 z)}e^{j\omega_1 t}\right]$$

where

$$k_{0i} = 2\pi/\lambda_{0i}.$$

The vector electric field amplitude is $\vec{E}_i= E_i\hat{e}_i$, where $\hat{e}_i$ is the unit polarization vectors in free-space. For p-polarized fields $\hat{e}_1 = \beta_1\hat{x} - \kappa_1\hat{z}, \hat{e}_2 = \beta_2\hat{x} + \kappa_2\hat{z}$, and $\hat{e}_3 = -\beta_3\hat{x} + \kappa_3\hat{z}$. For s-polarized fields $\hat{e}_i = \hat{y}$. The frequencies are related by $\omega_3 = \omega_1+\omega_2$, and the direction of the sum-frequency generated beam is determined by the momentum conservation condition

$$-k_{01}\kappa_1 + k_{02}\kappa_2 = k_{03}\kappa_3. \tag{1}$$

The nonlinear interaction at interfaces and thin films can be modeled by a polarization sheet $\vec{P}_S^{(2)}$ [48]. Following the formulism in [48]–[50], in the meter, kilogram, and second system, the electric field at the sum-frequency is $E(\omega_3) = j(k_3)/(2\beta_3)(\hat{e}_3\cdot \vec{F}_3 \cdot \vec{P}_S)$, and the intensity generated in free space, given by $I(\omega_3) = (1/2)\varepsilon_0 c\bar{E}(\omega_3)\bar{E}^*(\omega_3)$, is

$$I(\omega_3) = \frac{\omega_3^2}{2c^3\beta_3^2}\left|\chi_{\rm eff}^{(2)}\right|^2 I(\omega_1)I(\omega_2) \tag{2}$$

with the effective nonlinear susceptibility $\chi_{\rm eff}^{(2)} = (\hat{e}_3\cdot \vec{F}_3)\cdot \tilde{\chi}^{(2)} : (\hat{e}_1\cdot \vec{F}_1)(\hat{e}_2\cdot\vec{F}_2)$, where $\hat{e}_j$ is the unit polarization vectors defined previously and $F_x(\omega) = 1 - r_p^{123}(\omega), F_y(\omega) = 1 - r_s^{123}(\omega)$, and $F_z(\omega) = \varepsilon_1(r_p^{123}(\omega)+1)/\varepsilon_{\rm mono}$. The super and subscripts in the permittivity and reflectivity coefficients, i.e., 1, 2, and 3, refer to the air, the thin silicon dioxide layer, and silicon substrate, respectively. The reflectivity factors are

$$r_m^{123}(\omega) = \frac{r_m^{12}(\omega) + r_m^{23}(\omega)e^{-2jk_0\beta_{\rm SiO_2}d_{\rm SiO_2}}}{1 + r_m^{12}(\omega)r_m^{23}(\omega)e^{-2jk_0\beta_{\rm SiO_2}d_{\rm SiO_2}}} \tag{3}$$

where $m = s$, and $m = p$ correspond to the transverse electric and transverse magnetic polarization, respectively, and

$$r_p^{kl}(\omega) = \frac{\varepsilon_l(\omega)\beta^k - \varepsilon_k(\omega)\beta^l}{\varepsilon_l(\omega)\beta^k + \varepsilon_k(\omega)\beta^l} \tag{4a}$$

$$r_s^{kl}(\omega) = \frac{\beta^k - \beta^l}{\beta^k + \beta^l} \tag{4b}$$

where β^k refers to the z component of the wavevector in the kth layer.

V. Sum-Frequency in PBLG Films

We assume that the sum-frequency generation in the PBLG film dominates over any interfacial contributions, such that

$$\vec{P}_S^{(2){\rm Film}} = \varepsilon_0\chi_{\rm Film}^{(2)} :\vec{E}\ (\omega_2)\ \vec{E}\ (\omega_1). \tag{5}$$

The macroscopic tensor element is $\chi_{xyz}^{(2)} = N_s\langle(\hat{x}\cdot\hat{\xi})(\hat{y}\cdot\hat{\eta})(z\cdot\hat{\zeta})\rangle\alpha_{\xi\eta\zeta}^{(2)}$ where N_s is the surface density of the molecules and $(\hat{\xi},\hat{\eta},\hat{\zeta})$ is a right-handed coordinate system in the molecular frame. The second-order nonlinear optical susceptibility of the PBLG helix is modeled by a distribution of cylindrically shaped molecules around the a symmetry axis $\hat{\zeta}$, resulting in a cylindrical symmetry and only three independent tensor elements $\beta_{\zeta\zeta\zeta}^{(2)}$, and $\beta_{\xi\xi\zeta}^{(2)} = \beta_{\eta\eta\zeta}^{(2)}$ and $\beta_{\xi\zeta\xi}^{(2)} = \beta_{\zeta\xi\xi}^{(2)} = \beta_{\xi\zeta\xi}^{(2)} = \beta_{\zeta\xi\xi}^{(2)}$ [51]. Furthermore, in the PBLG SFG measurements, the visible and sum-frequency wavelengths are far from the electronic resonances, such that, compared to dominant $\beta_{\zeta\zeta\zeta}^{(2)}$, the contributions due to the elements $\beta_{\xi\zeta\xi}^{(2)} = \beta_{\zeta\xi\xi}^{(2)} = \beta_{\xi\zeta\xi}^{(2)} = \beta_{\zeta\xi\xi}^{(2)}$ are negligible. The IR interactions are resonantly enhanced when the polarization has a component along $\hat{\zeta}$. With such assumptions, the cylindrical symmetric molecule has only two nonvanishing elements: $\beta_{\zeta\zeta\zeta}^{(2)}$ and $\beta_{\xi\xi\zeta}^{(2)} = \beta_{\eta\eta\zeta}^{(2)}$. In the PBLG film, the molecules are tilted with respect to surface normal to produce an in-plane anisotropy. The tilt is described by a random variable θ, and distributed along an azimuthal angle ϕ, see Fig. 3. A

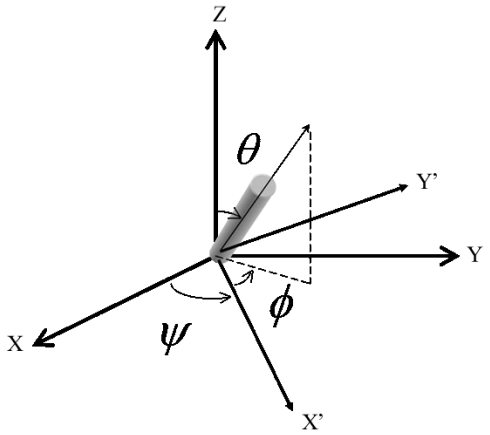

Fig. 3. Orientation of the PBLG helical axis is describe by the angles θ and ϕ in the X′Y′Z sample coordinate system. The angle ψ describes the rotation angle between the XYZ laboratory coordinate system and the X′Y′Z sample coordinate system.

Boltzman probability distribution function will be assumed for θ and a delta probability distribution function for ϕ.

With all the beams s-polarized (i.e., sss), the effective nonlinear susceptibility is

$$\begin{aligned}\chi_{\text{eff}}^{(2)sss} &= F_{Y3}F_{Y2}F_{Y1}\langle\sin\theta\rangle\sin\phi \\ &\quad\times(\beta_{\xi\xi\zeta}\langle\cos^2\theta\rangle\sin^2\phi+\beta_{\xi\xi\zeta}\cos^2\phi \\ &\quad+\beta_{\zeta\zeta\zeta}\langle\sin^2\theta\rangle\sin^2\phi). \end{aligned}\tag{6}$$

Note that $\chi_{\text{eff}}^{(2)sss}=0$ if the average tilt angle is zero, or the molecules are uniform distributed around the surface normal. As is expected, the sss-intensity is a very sensitive to the in-plane orientation of the PBLG molecules. The sss-intensity will have two distinct lobes that are perpendicular to the tilt-plane, which is defined by the angle ϕ.

With all the beams p-polarized (i.e., ppp), the effective nonlinear susceptibility is

$$\begin{aligned}\chi_{\text{eff}}^{(2)ppp} &= -L_{x3}\beta_3(L_{x\text{IR}}\beta_1\beta_{\xi\xi\zeta}\langle\cos^2\theta\rangle\cos^2\phi \\ &\quad+L_{x\text{IR}}\beta_1\beta_{\xi\xi\zeta}\sin^2\phi \\ &\quad+L_{x\text{IR}}\beta_1\beta_{\zeta\zeta\zeta}\cos^2\phi\langle\sin^2\theta\rangle) \\ &\quad+(L_{x2}\beta_2\cos\phi\langle\sin\theta\rangle+L_{z2}\kappa_2\langle\cos\theta\rangle) \\ &\quad\times L_{z1}(\beta_{\xi\xi\zeta}\kappa_1\cos\phi-\beta_{\zeta\zeta\zeta}\kappa_1\cos\phi)\langle\cos\theta\sin\theta\rangle \\ &\quad+L_{z3}\kappa_3(L_{x2}\beta_2\langle\sin\theta\rangle\cos\phi+L_{z2}\kappa_2\langle\cos\theta\rangle) \\ &\quad\times(L_{x1}\beta_1\beta_{\zeta\zeta\zeta}\langle\cos\theta\sin\theta\rangle\cos\phi \\ &\quad-L_{x1}\beta_1\beta_{\xi\xi\zeta}\langle\cos\theta\sin\theta\rangle\cos\phi \\ &\quad-L_{z1}\kappa_1\beta_{\xi\xi\zeta}\langle\sin^2\theta\rangle \\ &\quad-L_{z1}\kappa_1\beta_{\zeta\zeta\zeta}\langle\cos^2\theta\rangle). \end{aligned}\tag{7}$$

The sum-frequency intensity spectrum is described as [51]

$$\begin{aligned}I(\omega_3,\psi) &\propto \left|\chi_{\text{eff}}^{(2)}(\psi)\right|^2 \\ &= \left|A_{\text{NR}}(\psi)+\sum_n\frac{A_{Rn}(\psi)e^{j\varphi_n}}{\omega_{Rn}-\omega_3+j\Gamma_{Rn}}\right|^2 \end{aligned}\tag{8}$$

for the sample oriented at an azimuthal angle ψ, where $A_{Rn}(\psi),\Gamma_{Rn}$ and ω_{Rn} are the strength, damping constant, and angular frequency of a single resonant vibration, respectively. $A_{\text{NR}}(\psi)$ and φ_n are the nonresonant and the relative phase angle between the resonant and nonresonant signals. SFG vibrational spectroscopy identifies the resonant contributions in the monolayer.

VI. Experimental Methods

PBLG was grafted onto native silicon dioxide layers on silicon substrates by a vapor deposition polymerization reaction. The monomer, N-carboxy anhydride of γ-benzyl-L-glutamic acid (B-NCA), was spread at the bottom of a glass reactor. Onto the substrate (1-aminopropyl) triethoxysilane (APS) initiator was first deposited by immersing it in a 0.3 wt% APS in acetone for 1 h at 50 °C. The substrate was placed 1.5 cm above the B-NCA monomer and the chamber was evacuated and back-filled with N_2. The system was then heated to 105 °C and held at pressures of ca. 5×10^{-5} mbar for 2 h, during which the monomers in the vapor phase react with the surface-attached amino groups, which initiate a ring opening polymerization to form the PBLG film. After the reaction, the substrate was soaked in $1/9$ (v/v) of dichloroacetic acid/chloroform to remove physisorbed oligomers, leaving only chemically grafted PBLG on the surface.

The IR-visible SFG spectroscopy scans were measured made by spatially and temporally overlapping IR pulse and visible pulse in the PBLG film and detecting the sum-frequency signal in reflection. The visible light was produced by a frequency doubled Nd:YAG laser with 22-ps pulses at 10-Hz repetition rate (EKSPLA model PL2143C) whereas the infrared tunable light was produced by an OPG/OPA/DFG unit (EKSPLA PG501VIR/DFG). Using the synchronized frequency tripled output channel of the pump laser, generation of light in the wavelength range 0.42–2.3 μm was achieved using optical parametric generation and amplification in a LBO crystal. The idler was then used to seed the difference frequency generation in an AgGeSz cyrstal (DFG, between the seed and 1064 nm) achieving tuning in the 2.3–10 μm wavelength range. The system was delivering over 100 μJ between 2.5 and 5 μm while its line width was kept smaller than 6 cm^{-1}. The wavelength can be stepped in 1-nm increments in the region of interest under computer control.

The 0.532 μm laser beam was cleaned in a spatial filter, attenuated using a combination of a $\lambda/2$ plate and a polarizer, delayed and focused onto the sample to a size of 2.7 mm^2 resulting in an average fluence of 14 mJ/cm^2. A second $\lambda/2$ plate was used to set the polarization of the visible beam onto the sample. The IR polarization was set using a ZnSe rhomb coated for low Fresnel losses between 2.5 and 10 μm. A 25-mm lens focused the IR laser beam to a spot of 0.7 mm^2 on the sample leading a typical fluence of 10 mJ/cm^2 over the wavelength range 2.5–5 μm. The IR beam is focused within the larger visible spotsize. The sum-frequency is generated in the overlap region. A HeNe laser beam was set collinear to the infrared laser beam to ease the alignment.

The angle between the incident infrared and visible laser beams was kept constant at 90° and the detection set at 25° with respect to the IR beam. While scanning the IR wavelength, the sample was rotated such that the phase matching condition was maintained, and the sum-frequency beam remains at a constant position on the detector.

The sum-frequency signal is filtered by a set of sharp cut edge color filters (Edmund Scientific, #J30 635, blue additive dichroic filter 4×10^{-3} at 0.532 μm and >90% transmission in the 0.400–0.495-μm sum-frequency wavelength range). An additional interference filter (Notch-Plus, Kaiser Optical system, Inc.) was used to attenuate any stray 0.532-μm radiation by OD6. A photomultiplier (Hamamatsu #6095) with high responsivity in the blue range was used to detect signals. The produced current was transformed via a 50-Ω resistance and the signal was preamplified using a 300-MHz preamplifier (Quad SR445). The data were analyzed using a gated integrator (SR250). The boxcar average was performed in baseline subtraction mode to reduce the background noise floor. Data was digitized (SRS245) and transferred to a computer.

The orientation of the PBLG on the surfaces is mapped by, for a fixed set of the input polarizations, scanning the sample to a point in the xy plane and at each point rotating the sample around the boundary normal about an azimuthal angle ψ through 360°. All translation and rotation stages are under computer control.

An ellipsometer (Gaertner Scientific Corp., L116C) with a He-Ne laser was used to measure film thickness of the PBLG layer. A refractive index of $\sqrt{\varepsilon_{r\mathrm{PBLG}}} = 1.48$ was used for all the measurements and calculations. The reported film thickness was averaged from at least five different spots on each sample.

Fourier transform IR (FTIR) spectral measurements (Perkin-Elmer Spectrum 2000) were taken in transmission mode with a mercury cadmium telluride nitrogen cooled detector. For each sample, 1064 scans were taken at a resolution of 4 cm^{-1}.

The film morphology was probed using a atomic force microscope (Digital Instruments, NanoScope IIIa MultiMode) and the images were captured in the tapping mode using E and J scanners at frequencies of 0.5–1 Hz.

VII. Results and Discussion

Fig. 4 shows the infrared transmission spectra of the endgrafted PBLG film. The peptides in the helix produce vibrational signatures due to the stretches of N-H (amide A, 3294 cm^{-1}), C-N (amide II, 1549 cm^{-1}), and C = O (amide I, 1653 cm^{-1}) segments. The peak at 1734 cm^{-1} is the side chain C = O peak arising from the ester group. The peaks at 3070 cm^{-1} are the three aromatic CH stretches. Around 3100 cm^{-1}, there is an Amide B peak (from the overtone of the amide II vibration) that is obscured by the aromatic bands. The peak at 2968 cm^{-1} is the methylene stretch (CH_2-CH_2 stretch). The spectral features below ~1300 cm^{-1} are caused by overtones, bends, and scissors of various molecules. The IR vibrational signatures are consistent with [43].

Fig. 5 shows the sum-frequency reflection spectra of the endgrafted PBLG film when all beams are p polarized. The main peaks in this spectrum correspond to stretches of N-H (amide A, 3294 cm^{-1}) and the C = O (amide I, 1653 cm^{-1}) segments. In organic molecules, the second-order hyperpolarizability β is maximized by efficient intramolecular charge transfer (ICT) of delocalized electrons between donor and acceptor groups. Within each peptide unit the intramolecular charge transfer is poor and the β associated with each peptide is comparable to small molecules [3]. At a supramolecular level, the β is several times larger than each peptide unit, not because of ICT, but due to the number of NH and CO-groups units that are well-oriented in α-helix. As seen in Fig. 1, the NH and CO-groups organize in a noncentrosymmetric manner within the molecular helical scaffold. As seen in Fig. 1, the C = O group repeat unit i forms a hydrogen bond with the N-H group repeat unit $i + 4$, and

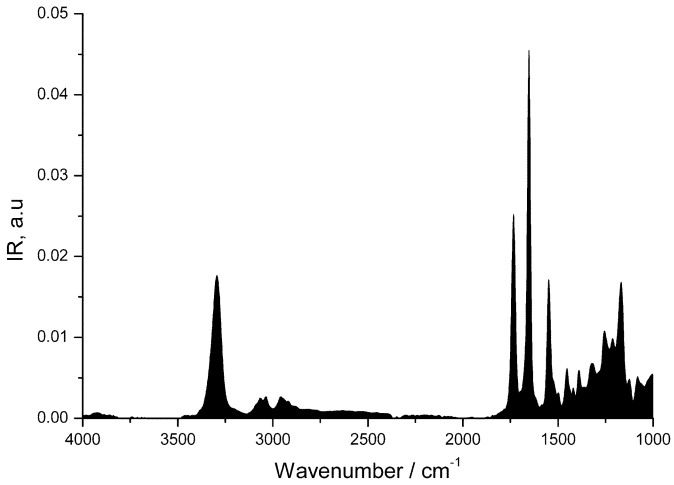

Fig. 4. IR transmission spectrum of endgrafted PBLG film. The peaks assignments are N-H (amide A, 3294 cm^{-1}), C-N (amide II, 1549 cm^{-1}), C = O (amide I, 1653 cm^{-1}) and a side chain C = O peak (1734 cm^{-1}) arising from the ester group.

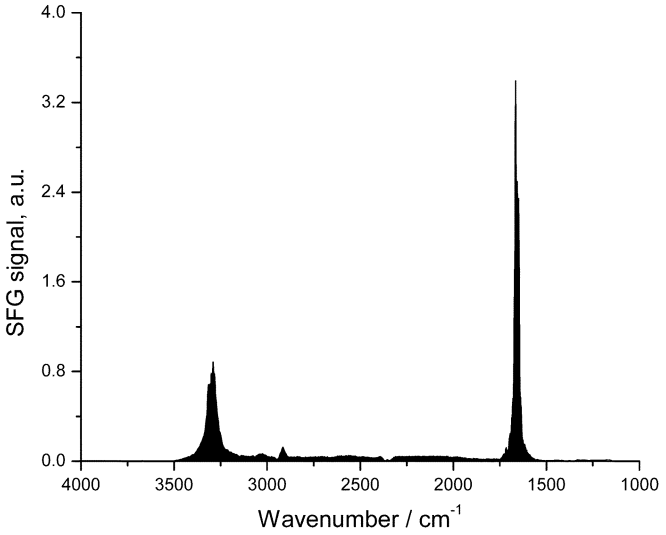

Fig. 5. Sum-frequency spectrum of endgrafted PBLG film with all beam p polarized. The two main peaks correspond to ths stretches of N-H (amide A, 3294 cm^{-1} region) and C = O (amide I, 1653 cm^{-1} region) segments. The main peaks in the sum-frequency spectrum originate from collective radiation from noncentrosymmetric oriented NH and CO-groups within a single helix, and their noncentrosysmmetric organization of the helices within the film. The amide II band and other features clearly present in the IR spectra are notably absent in the sum-frequency spectrum because they do not have noncentrosymmetric order.

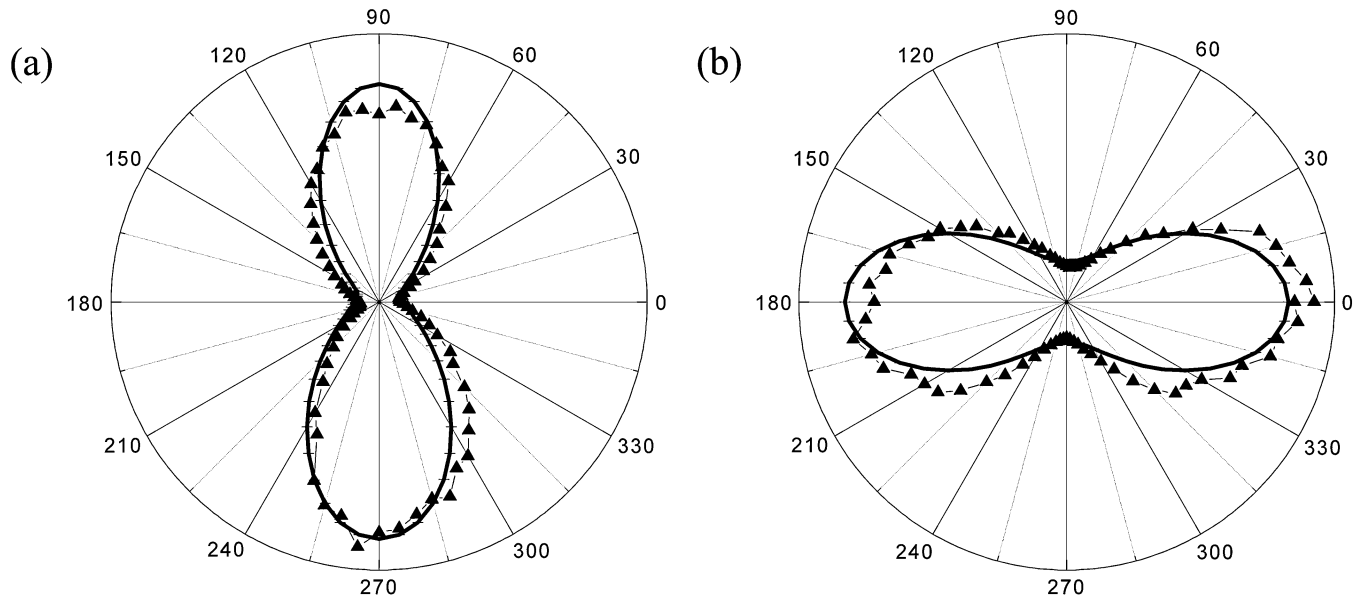

Fig. 6. Experimental measurement (dotted curve) and the theoretical fitting result (solid curve) for (a) all beams p polarized, and (b) all beams s polarized for measurements taken on the N-H stretch (amide A, 3294 cm^{-1}). The location of the point on the sample is $x = 5.0$, $y = 0.5$ mm.

are organized in a noncentrosymmetric manner within a rigid α-helical molecular scaffold. There is no ICT between the ith C = O group and the $(i+4)$th N-H group, each peptide unit acts as an independent radiator. In the endgrafted PBLG film the individual PBLG helices are well-oriented with respect to each other due to a repulsive intersupramolecular electrostatic repulsive force. Each PBLG is grafted to the substrate through the same end-terminus, leaving an array of right-handed helices, each with a very large electrostatic dipole moment pointing in the same direction. The main peaks in the sum-frequency spectrum originate from collective radiation from noncentrosymmetric oriented NH and CO-groups within a single helix, and the noncentrosymmetric organization of the helices in the film. The amide II band and other features clearly present in the IR spectra are notably absent because they do not have noncentrosymmetric order. For example, the C-N (amide II) peak present in the IR spectrum is absent in the sum-frequency spectra, because as can be seen in Fig. 1, the C-N groups are centrosymmetrically organized within the helix.

The PBLG films were remarkably thermally stable. The samples were heated to about 150°C while *in-situ* SFG spectra measurements were performed. Up to about 130 °C no changes in the spectra were observed. At higher temperature the peaks disappeared without observing a broadening of the peaks, which is indicative of PBLG molecules being sublimated from the surface before thermal disorder sets in. This stability of PBLG films to 130 °C has also been independently confirmed by *in situ* AFM studies [52].

The average orientation of the helices was determined by fixing the IR wavelength to the the N-H (amide A, 3294 cm^{-1}) stretch and then rotating the sample around a fixed point while keeping the polarizations fixed at either ppp or sss. A nonlinear least square fit was performed using the effective nonlinear susceptibilities given by (6) and (7). The fitting parameters are θ, ϕ, and $r = \beta_{\xi\xi\zeta}/\beta_{\zeta\zeta\zeta}$. The angle ϕ is estimated from the two distinct lobes in sss-polar that are perpendicular to the tilt-plane Using this value for ϕ, the average tilt angle θ is determined from the ppp-polar measurements. The following parameters were used for the Fresnel factors. The indexes of refraction for the silicon substrate are $\sqrt{\varepsilon_{r\mathrm{Si}}} = 4.14 + j0.045$ at 0.532 μm (the wavelength of the visible beam), $\sqrt{\varepsilon_{r\mathrm{Si}}} = 4.522 + j0.134$ at 0.465 μm (the wavelength of the sum frequency component), and $\sqrt{\varepsilon_{r\mathrm{Si}}} \approx 3.43$ at 3.7 μm (the wavelength of the IR beam). The silicon dioxide was 30 nm thick and the indexes of refraction are $\sqrt{\varepsilon_{r\mathrm{SiO_2}}} = 1.461$ at 0.532, $\sqrt{\varepsilon_{r\mathrm{SiO_2}}} = 1.465$ at 0.465, and $\sqrt{\varepsilon_{r\mathrm{SiO_2}}} = 1.400$ at 3.7 μm. The index of monolayer was set to 1.48, since the fitted value for θ changed by less than 3% when the index of refraction of the monolayer was in 1.43–1.50 range. For the ppp-polar measurement, the value of r fitted to $1/3.2 < r < 1/3.1$. The silicon dioxide layer is so thin compared to any of the wavelengths present, and thus has minimal effect on the Fresnel factors. Fig. 6 shows the fitting result of one of the measurements. Fig. 7 shows five polar measurements and their location on the sample and their nonlinear least square fits. Table I summarizes the average angle θ and ϕ for the five points. The average value of the tilt angle is $\langle\theta\rangle = 58.38 \pm 8.75°$ which compares well with the IR tilt angle measurements of PBLG films $\langle\theta\rangle = 58 \pm 5°$ measured by Wieringa *et al.* [43].

The orientation distribution of the PBLG molecules on the sample was imaged using sum-frequency from the N-H band in the following manner. Imaging the surface by performing ppp and sss polar measurements on a closely spaced grid is impractical since to accumulate such dataset at each sample point takes more than one hour. To overcome this practical limitation, we set the beams at either ppp or sss, and scan the sample in the xy-plane on a 4×4 mm grid, with points spaced 63 μm apart. Fig. 8 shows the high spatial resolution sss- and ppp- datasets of the SFG signal intensity distribution on the sample. The orientation distribution of the helix within 4×4 mm^2 region is determined at a specific point by using the information in the five higher angle resolution ppp- and sss-polar datasets (Fig. 7) and the information in the higher spatial resolution ppp- and sss-xy

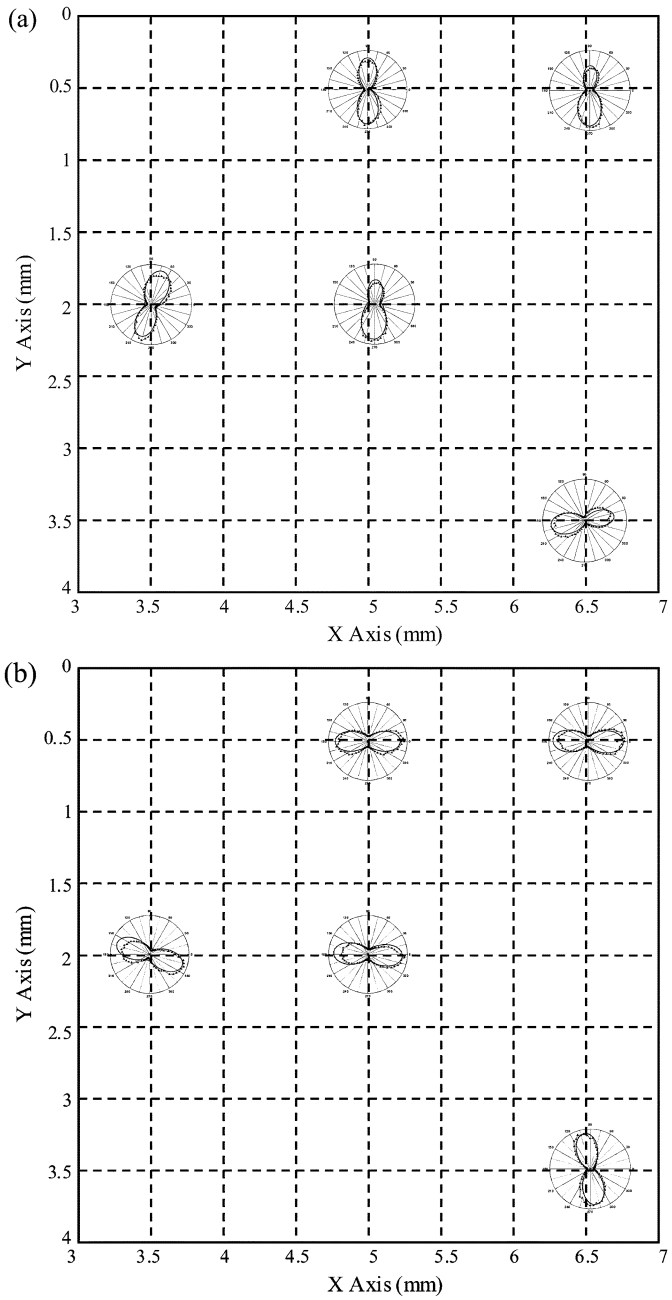

Fig. 7. Polar measurements for (a) all beams p polarized and (b) all beams s polarized taken on the N-H stretch (amide A, 3294 cm^{-1}) with their coordinates shown in the grid.

TABLE I
AVERAGE TILT AND AZIMUTHAL ANGLE MEASUREMENTS AT POINTS ON THE SAMPLE

θ	ϕ	xy-coordinate
58.44 °	0 °	(6.5, 3.5) mm
48.38 °	96.43 °	(5.0, 2.0) mm
61.91 °	90.61 °	(5.0, 0.5) mm
64.26 °	108.25 °	(3.5, 2.0) mm
49.51 °	92.04°	(6.5, 0.5) mm

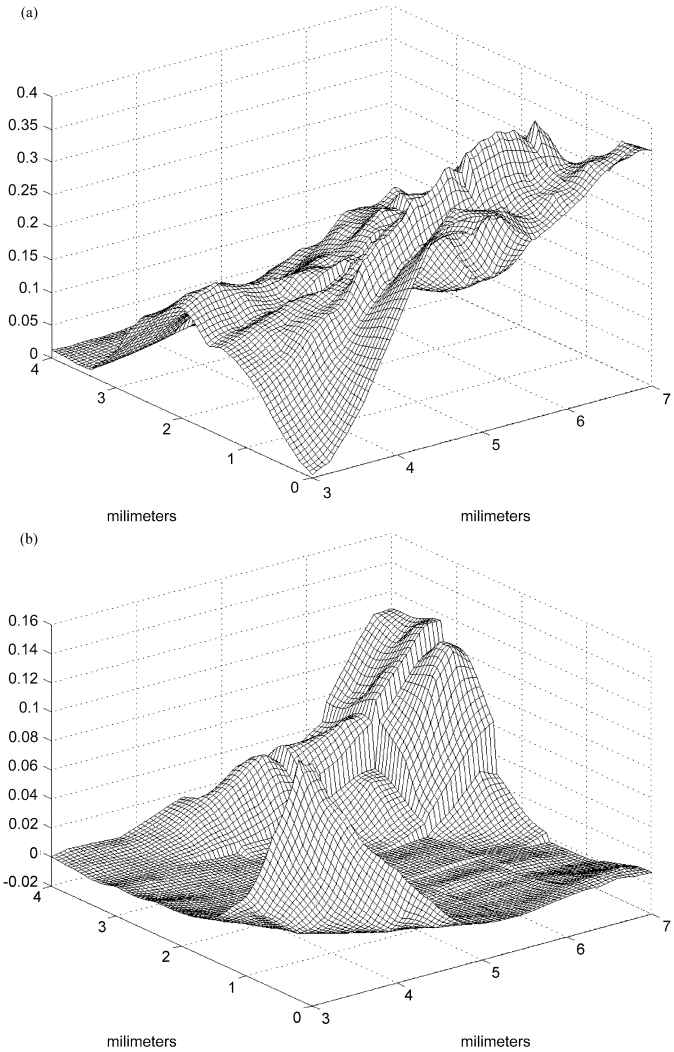

Fig. 8. Sum-frequency xy measurements for (a) all beams p polarized, and (b) all beams s polarized taken on the N-H stretch (amide A, 3294 cm^{-1}). The measurement points are spaced 63 μm apart.

datasets (Fig. 8). From the sss- and ppp-xy datasets, the known SFG intensities at the point (i, j) at coordinate 'x' and 'y' are

$$I_{sss}(\theta_{ij},\phi_{ij}) \propto \left|\chi_{\text{eff}}^{(2)sss}(\theta_{ij},\phi_{ij})\right|^2$$

and

$$I_{ppp}(\theta_{ij},\phi_{ij}) \propto \left|\chi_{\text{eff}}^{(2)ppp}(\theta_{ij},\phi_{ij})\right|^2$$

where θ_{ij} ar ϕ_{ij} are the unknown angles. Let the coordinate of the nearest point where polar measurements were performed be (x_p, y_p). From the sss- and ppp-polar datasets, we have its intensity

$$I_{sss}(\theta_p,\phi_p) \propto \left|\chi_{\text{eff}}^{(2)sss}(\theta_p,\phi_p)\right|^2$$

and

$$I_{ppp}(\theta_p,\phi_p) \propto \left|\chi_{\text{eff}}^{(2)ppp}(\theta_p,\phi_p)\right|^2$$

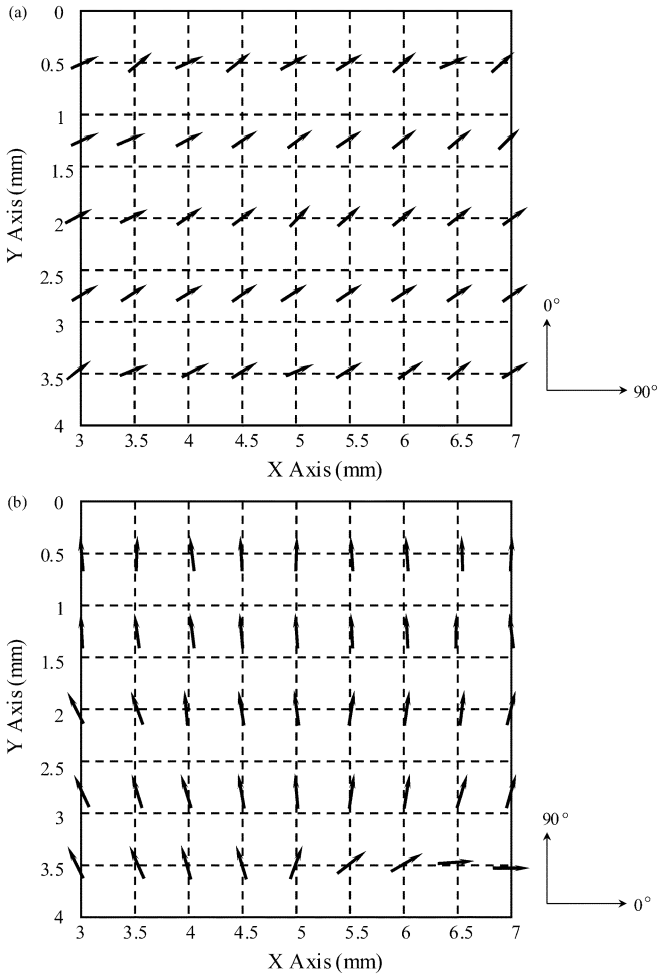

Fig. 9. Distribution of the (a) out-plane and (b) in-plane orientation of the PBLG molecules.

where θ_p and ϕ_p are known, see Table I. The angle θ_{ij} and ϕ_{ij} are then numerically solved from the following nonlinear equations:

$$\frac{I_{sss}(\theta_{ij},\phi_{ij})}{I_{sss}(\theta_p,\phi_p)} = \frac{\left|\chi_{\text{eff}}^{(2)sss}(\theta_{ij},\phi_{ij})\right|^2}{\left|\chi_{\text{eff}}^{(2)sss}(\theta_p,\phi_p)\right|^2} \tag{9a}$$

$$\frac{I_{ppp}(\theta_{ij},\phi_{ij})}{I_{ppp}(\theta_p,\phi_p)} = \frac{\left|\chi_{\text{eff}}^{(2)sss}(\theta_{ij},\phi_{ij})\right|^2}{\left|\chi_{\text{eff}}^{(2)ppp}(\theta_p,\phi_p)\right|^2}. \tag{9b}$$

In this numerical solution, the value of θ is confined to the range $40^\circ \leq \theta \leq 70^\circ$ to resolve multivalued solutions. Fig. 9 shows the spatial map of the tilt angle and the azimuthal orientation. The distribution of the out of plane tilt angle is very homogeneous over the measured area. Similarly, so is the distribution of the in plane azimuthal angle, with the exception of a transition by 90° in one of the corners. This is indicative of the formation of electrostatic domains as large in area as several millimeters square.

The morphology of end-grafted PBLG monolayers on silicon dioxide substrates has been investigated [46], [52]. A representative AFM image of an endgrafted PBLG film is shown in Fig. 10 over a 5 $\times$ 5 μm area. The chemisorbed PBLG surface has a whispylike appearance with no indication of grains. The surface does not have the fibrillar and network structure observed in physisorbed PBLG films, and is not granular as was found with other chemisorbed polypeptide films. The SFG mapping of the orientation of the helices suggest that in the chemisorbed films uniform domains exist that are on the order of several millimeters in size.

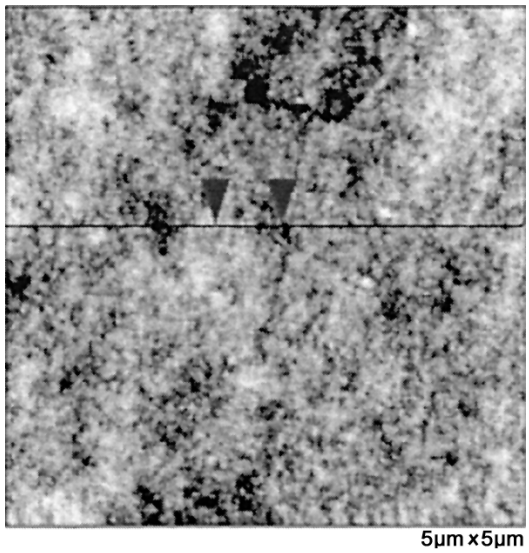

Fig. 10. Atomic force image of a endgrafted chemi-absorbed PBLG monolayer filom over a 5 $\times$ 5 μm area. Reproduced from [52] with permission.

VIII. Conclusion

We have shown experimentally for the first time, by sum-frequency spectroscopy, that the origins of the optical second-order nonlinearity in PBLG molecules are collective contributions from the amide N-H (amide A, 3294 cm^{-1}) and the C = O (amide I, 1653 cm^{-1}) segments. Hydrogen bonding creates an α-helix, and also organizes the N-H and C = O segments in a noncentrosymmetric manner. Not only does this organization in each α-helix lead to a large electrostatic dipole moment per supramolecule, it also causes the large second-order nonlinear hyperpolarizibility β per supramolecule. In the endgrafted chemi-absorbed monolayers, an ensemble of molecules is highly organized over a large area because of the large electrostatic repulsive forces caused by dipole-dipole interaction and parallel alignment between neighboring supramolecules. By scanning sum-frequency imaging, we showed that the orientation of the helical molecules is uniform over several millimeters. Considering the diameter of the PBLG helix is on the order of 3 nm, the thickness of the film is 30 nm, the uniformity of the orientation over length scale of several millimeters is remarkable and indicative of how effectively protein structures can self-organize.

References

[1] K. E. Rieckhoff and W. J. Peticolas, "Optical second-harmonic generation in crystalline amino acids," *Science*, vol. 147, pp. 610–611, 1965.
[2] S. F. W. P. Hansen, "Optical second harmonic generation in biological systems," *Appl. Opt.*, vol. 10, pp. 2350–2353, 1971.

[3] B. F. Levine and C. G. Bethea, "2nd order hyperpolarizability of a polypeptide alpha-helix—Poly-gamma-benzyl-L-glutamate," *J. Chemi. Phys.*, vol. 65, pp. 1989–1993, 1976.

[4] B. F. Levine and C. G. Bethea, "2nd and 3rd order hyperpolarizabilities of organic-molecules," *J. Chem. Phys.*, vol. 63, pp. 2666–2682, 1975.

[5] A. C. Millard, P. J. Campagnola, W. Mohler, A. Lewis, and L. M. Loew, "Second harmonic imaging microscopy," *Biophoton. B*, vol. 361, pp. 47–69, 2003.

[6] P. J. Campagnola and L. M. Loew, "Second-harmonic imaging microscopy for visualizing biomolecular arrays in cells, tissues, and organizms," *Nature Biotechnol.*, vol. 21, pp. 1356–1360, 2003.

[7] T. Rasing, J. Huang, A. Lewis, T. Stehlin, and Y. R. Shen, "Insitu determination of induced dipole-moments of pure and membrane-bound retinal chromophores," *Phys. Rev. A, Gen. Phys.*, vol. 40, pp. 1684–1687, 1989.

[8] L. Moreaux, O. Sandre, and J. Mertz, "Membrane imagind by second-harmonic generation microscopy," *J. Opt. Soc. Amer. B, Opt. Phys.*, vol. 17, pp. 1685–1694, 2000.

[9] P. J. Campagnola, M. D. Wei, A. Lewis, and L. M. Loew, "High-resolution nonlinear optical imaging of live cells by second harmonic generation," *Biophys. J.*, vol. 77, pp. 3341–3349, 1999.

[10] P. J. Campagnola, H. A. Clark, W. A. Mohler, A. Lewis, and L. M. Loew, "Second-harmonic imaging microscopy of living cells," *J. Biomed. Opt.*, vol. 6, pp. 277–286, 2001.

[11] S. Roth and I. Freund, "2nd harmonic-generation in collagen," *J. Chem. Phys.*, vol. 70, pp. 1637–1643, 1979.

[12] ——, "Coherent optical harmonic-generation in rat-tail tendon," *Opt. Commun.*, vol. 33, pp. 292–296, 1980.

[13] ——, "Optical 2nd-harmonic scattering in rat-tail tendon," *Biopolymers*, vol. 20, pp. 1271–1290, 1981.

[14] ——, "2nd harmonic-generation and orientational order in connective-tissue—A mosaic model for fibril orientational ordering in rat-tail tendon," *J. Appl. Crystallogr.*, vol. 15, pp. 72–78, 1982.

[15] I. Freund, M. Deutsch, and A. Sprecher, "Connective-tissue polarity-optical 2nd-harmonic microscopy, crossed-beam summation, and small-angle scattering in rat-tail tendon," *Biophys. J.*, vol. 50, pp. 693–712, 1986.

[16] L. Moreaux, O. Sandre, S. Charpak, M. Blanchard-Desce, and J. Mertz, "Coherent scattering in multi-harmonic light microscopy," *Biophys. J.*, vol. 80, pp. 1568–1574, 2001.

[17] A. C. Millard, P. J. Campagnola, W. Mohler, A. Lewis, and L. M. Loew, "Second harmonic imaging microscopy," *Biophotonics*, pt. B, vol. 361, pp. 47–69, 2003.

[18] P. Stoller, K. M. Reiser, P. M. Celliers, and A. M. Rubenchik, "Polarization-modulated second harmonic generation in collagen," *Biophys. J.*, vol. 82, pp. 3330–3342, 2002.

[19] P. Stoller, B. M. Kim, A. M. Rubenchik, K. M. Reiser, and L. B. Da Silva, "Polarization-dependent optical second-harmonic imaging of a rat-tail tendon," *J. Biomed. Opt.*, vol. 7, pp. 205–214, 2002.

[20] P. Stoller, P. M. Celliers, K. M. Reiser, and A. M. Rubenchik, "Quantitative second-harmonic generation microscopy in collagen," *Appl. Opt.*, vol. 42, pp. 5209–5219, 2003.

[21] C. Bosshard, K. Sutter, P. Pretre, J. Hulliger, M. Florsheimer, P. Kaatz, and P. Gunter, *Organic Nonlinear Optical Materials*. Basel, Switzerland: Gordon and Breach, 1995, vol. 1.

[22] M. G. Kuzyk, *Characterization Techniques and Tabulations for Organic Nonlinear Optical Materials*. New York: Marcel Dekker, 1998.

[23] S. R. Marder, J. W. Perry, and W. P. Schaefer, "Synthesis of organic salts with large 2nd-order optical nonlinearities," *Science*, vol. 245, pp. 626–628, 1989.

[24] H. Kuhn and D. Mobius, "Systeme aus Monomolekularen Schicten-Zusamenbau and chemische Verhalten," *Angew. Chem.*, vol. 83, pp. 672–690, 1971.

[25] G. Decher, *Multilayer Thin Films*. New York: Wiley-VCH, 2003.

[26] G. Decher and J. D. Hong, "Buildup of ultrathin multilayer films by a self-assembly process. 1. Consecutive adsorption of anionic and cationic bipolar amphiphiles on charged surfaces," *Makromolekulare Chemie-Macromolecular Symposia*, vol. 46, pp. 321–327, 1991.

[27] G. Decher, J. D. Hong, and J. Schmitt, "Buildup of ultrathin multilayer films by a self-assembly process. 3. Consecutively alternating adsorption of anionic and cationic polyelectrolytes on charged surfaces," *Thin Solid Films*, vol. 210, pp. 831–835, 1992.

[28] F. Kajzar, K. S. Lee, and A. K. Y. Jen, "Polymeric materials and their orientation techniques for second-order nonlinear optics," *Adv. Polymer Sci.*, vol. 161, pp. 1–85, 2003.

[29] X. D. Zhu, H. Suhr, and Y. R. Shen, "Surface vibrational spectroscopy by infrared-visible sum frequency generation," *Phys. Rev. B, Condens. Matter*, vol. 35, pp. 3047–3050, 1987.

[30] C. D. Bain, "Sum-frequency vibrational spectroscopy of the solid-liquid interface," *J. Chem. Soc.-Faraday Trans.*, vol. 91, pp. 1281–1296, 1995.

[31] J. Wang, S. M. Buck, and Z. Chen, "The effect of surface coverage on conformation changes of bovine serum albumin molecules at the air-solution interface detected by sum frequency generation vibrational spectroscopy," *Analyst*, vol. 128, pp. 773–778, 2003.

[32] ——, "Sum frequency generation vibrational spectroscopy studies on protein adsorption," *J. Phys. Chem. B*, vol. 106, pp. 11 666–11 672, 2002.

[33] J. Wang, S. M. Buck, M. A. Even, and Z. Chen, "Molecular responses of proteins at different interfacial environments detected by sum frequency generation vibrational spectroscopy," *J. Amer. Chem. Soc.*, vol. 124, pp. 13 302–13 305, 2002.

[34] Y. C. Chang, C. W. Frank, G. G. Forstmann, and D. Johannsmann, "Quadrupolar and polar anisotropy in end-grafted alpha-helical poly(gamma-benzyl-L-glutamate) on solid substrates," *J. Chem. Phys.*, vol. 111, pp. 6136–6143, 1999.

[35] T. Verbiest, C. Samyn, C. Boutton, S. Houbrechts, M. Kauranen, and A. Persoons, "Second-order nonlinear optical properties of a chromophore-functionalized polypeptide," *Adv. Mater.*, vol. 8, pp. 756–759, 1996.

[36] A. W. Harper, S. Sun, L. R. Dalton, S. M. Garner, A. Chen, S. Kalluri, W. H. Steier, and B. H. Robinson, "Translating microscopic optical nonlinearity into macroscopic optical nonlinearity: The role of chromophore-chromophore electrostatic interactions," *J. Opt. Soc. Amer. B—Opt. Phys.*, vol. 15, pp. 329–337, 1998.

[37] H. Block and C. P. Shaw, "2nd-harmonic generation in poly(alpha-amino acid) and poly(isocyanate) films," *Polymer*, vol. 33, pp. 2459–2462, 1992.

[38] Z. Tokarski, L. V. Natarajan, B. L. Epling, T. M. Cooper, K. L. Hussong, T. M. Grinstead, and W. W. Adams, "Nonlinear-optical characterization of chromophore-modified poly[L-glutamate] thin-films," *Chem. Mater.*, vol. 6, pp. 2063–2069, 1994.

[39] Y. C. Chang and C. W. Frank, "Grafting of poly(gamma-benzyl-L-glutamate) on chemically modified silicon oxide surfaces," *Langmuir*, vol. 12, pp. 5824–5829, 1996.

[40] J. K. Whitesell and H. K. Chang, "Directionally aligned helical peptides on surfaces," *Science*, vol. 261, pp. 73–76, 1993.

[41] R. H. Wieringa and A. J. Schouten, "Oriented thin film formation by surface graft polymerization of gamma-methyl L-glutamate N-carboxyanhydride in the melt," *Macromolecules*, vol. 29, pp. 3032–3034, 1996.

[42] R. H. Wieringa, E. A. Siesling, P. F. M. Geurts, P. J. Werkman, E. J. Vorenkamp, V. Erb, M. Stamm, and A. J. Schouten, "Surface grafting of poly(L-glutamates). 1. Synthesis and characterization," *Langmuir*, vol. 17, pp. 6477–6484, 2001.

[43] R. H. Wieringa, E. A. Siesling, P. J. Werkman, H. J. Angerman, E. J. Vorenkamp, and A. J. Schouten, "Surface grafting of poly(L-glutamates). 2. Helix orientation," *Langmuir*, vol. 17, pp. 6485–6490, 2001.

[44] R. H. Wieringa, E. A. Siesling, P. J. Werkman, E. J. Vorenkamp, and A. J. Schouten, "Surface grafting of poly(L-glutamates). 3. Block copolymerization," *Langmuir*, vol. 17, pp. 6491–6495, 2001.

[45] A. Heise, H. Menzel, H. Yim, M. D. Foster, R. H. Wieringa, A. J. Schouten, V. Erb, and M. Stamm, "Grafting of polypeptides on solid substrates by initiation of N-carboxyanhydride polymerization by amino-terminated self-assembled monolayers," *Langmuir*, vol. 13, pp. 723–728, 1997.

[46] Y. C. Chang and C. W. Frank, "Vapor deposition-polymerization of alpha-amino acid N-carboxy anhydride on the silicon(100) native oxide surface," *Langmuir*, vol. 14, pp. 326–334, 1998.

[47] T. Jaworek, D. Neher, G. Wegner, R. H. Wieringa, and A. J. Schouten, "Electromechanical properties of an ultrathin layer of directionally aligned helical polypeptides," *Science*, vol. 279, pp. 57–60, 1998.

[48] T. F. Heinz, *Second-Order Nonlinear Optical Effects at Nonlinear Surfaces*. Amsterdam, The Netherlands: Elsevier, 1991, vol. 29.

[49] X. Wei, X. W. Zhuang, S. C. Hong, T. Goto, and Y. R. Shen, "Sum-frequency vibrational spectroscopic study of a rubbed polymer surface," *Phys. Rev. Lett.*, vol. 82, pp. 4256–4259, 1999.

[50] Y. R. Shen, "Surface spectroscopy by nonlinear optics," in *Frontiers in Laser Spectroscopy, Proceedings of the International School of Physics Enrico Fermi*, T. W. Hansch and M. Inguscio, Eds. Amsterdam, The Netherlands: North Holland, 1994, pp. 139–159.

[51] X. Zhuang, P. B. Miranda, D. Kim, and Y. R. Shen, "Mapping molecular orientation and conformation at interfaces by surface nonlinear optics," *Phys. Rev. B, Condens. Matter*, vol. 59, pp. 12 632–12 640, 1999.

[52] N. H. Lee, L. M. Christensen, and C. W. Frank, "Morphology of vapor-deposited poly(alpha-amino acid) films," *Langmuir*, vol. 19, pp. 3525–3530, 2003.

André Knoesen (S'83–M'87–SM'92) was born in South Africa in 1958. He received the B.Ing. degree in electronic engineering from the University of Pretoria, Pretoria, South Africa, in 1980 and the M.S.E.E. and Ph.D. degrees from the Georgia Institute of Technology, Atlanta, in 1982 and 1987, respectively.

He joined the Department of Electrical Engineering, University of California, Davis, in 1987, and he is now a Professor. He performs research in materials and devices for high-frequency electronic and optoelectronic applications. The focus of his research is organic thin films.

Dr. Knoesen is a Fellow of the Optical Society of America. He has served in various capacities on the IEEE LEOS Conference, Nonlinear Optics Subcommittee, from 1994 to the present.

Saulius Pakalnis received the M.S. and Ph.D. degrees in physics from the Vilnius University, Vilnius, Lithuania, in 1984 and 1993, respectively.

He performed postdoctoral research at the Department of Physical Chemistry, University of Jyvaskyla, Jyvaskyla, Finland, in 1995; at the Laboratory of Molecular Compounds Physics, Institute of Physics, Vilnius, from 1996 to 1998; at the Department of Medical and Physical Engineering, University of Applied Sciences, Jena, Germany, from 1998 to 1999; at the Department of Electrical and Computer Engineering, University of California, Davis, in 2000; and at the Department of Chemistry, Virginia Commonwealth University, Richmond, from 2001 to 2002. He is currently the owner of RST Company, Vilnius.

Mingshi Wang received the B.S. degree from the Department of Electrical Engineering and Information Science, University of Science and Technology of China, Hefei, in 2001, and the M.S. degree in 2003 from the Department of Electrical and Computer Engineering, University of California, Davis, where he is currently working toward the Ph.D. degree.

His research interests include imaging using nonlinear optics techniques such as sum frequency generation and second harmonic generation.

W. D. Wise was born in San Francisco, CA, in 1979. He received the B.A. degree in physics and in engineering sciences from Harvard University, Cambridge, MA, in 2002. He is working toward the Ph.D. degree at the Department of Physics, Massachusetts Institute of Technology, Cambridge, MA.

As an undergraduate, he performed research as a Center on Polymer Interfaces Undergraduate Research Fellow in 2000 and as a Department of Energy Undergraduate Fellow in 2001. His current research interests include nanoscale investigations of high-temperature superconductors.

N. Lee, photograph and biography not available at the time of publication.

Curt W. Frank was born in Minnesota in 1945. He received the B.Chem.E. degree in chemical engineering from the University of Minnesota, Minneapolis, in 1967, and the M.S. and Ph.D. degrees in chemical engineering from the University of Illinois Urbana, in 1969 and 1972, respectively.

He was with Sandia National Laboratories, Albuquerque, NM, for four years and then joined the Department of Chemical Engineering, Stanford, Stanford, CA, in 1976, where he is currently a Professor and Department Chair. His research interests include the interface science of soft materials.

Dr. Frank is a Fellow of the American Physical Society. He was Chair of the Polymer Chemistry Division, American Chemical Society, in 1993.